AR-001-415

DEPARTMENT OF DEFENCE

DEFENCE SCIENCE AND TECHNOLOGY ORGANISATION

ELECTRONICS RESEARCH LABORATORY

TECHNICAL REPORT

ERL-0046-TR

AN IMPROVED IONOSPHERIC IRREGULARITY MODEL

D. G. Singleton

S U M M A R Y

Modifications are made to the global model developed by Fremouw et al. for the incremental electron density of F-layer irregularities in order to force the model into agreement with a considerable body of scintillation and spread-F data. While special attention is given to the equatorial region, where the original model was particularly lacking, the results of other studies are used to update the model in the other latitude regions and so provide a model of general application. The model now embodies the effect of magnetic activity at all latitudes, variations of occurrence with longitude in the equatorial region, variability of the width and position of the equatorial region, the influence of irregularity layer thickness, irregularity shape and electron density power spectrum, as well as the diurnal, seasonal and sunspot cycle variations of irregularity occurrence and strength at all latitudes. The improvements proposed not only enhance the model's usefulness as a simulation technique in engineering applications, but should also provide an impetus to the understanding of the physics of the irregularities.

POSTAL ADDRESS: Chief Superintendent, Electronics Research Laboratory, Box 2151, G.P.O., Adelaide, South Australia, 5001.

TABLE OF CONTENTS

LIST OF FIGURES

1. INTRODUCTION

Fremouw and Bates(ref.1) and later Fremouw and Rino(ref.2) were the first to attempt to produce an irregularity model by collating the data available in the literature on the occurrence, strength, size, etc. of F-region ionization density irregularities. They proposed an empirical model of global scintillation behaviour taking into account variations due to time of day, season, sunspot-cycle phase and latitude. An extension of this model to allow simulation of spread-F occurrence as well as scintillation index was proposed by Singleton(ref.3). This spread-F adaption of the model was used subsequently to better define the sunspot cycle dependence of the model(ref.4). The need for the model to allow for the effects which magnetic activity have on the behaviour of the irregularities was first addressed by Pope(ref.5). He proposed a modification to the model to achieve this at high latitudes. This paper indicates how the model can be further modified so as to allow the simulation of the effect of magnetic activity on the irregularities at the low latitudes. It also considers a further effect, hitherto neglected in the modelling process, namely variations in irregularity occurrence with longitude.

The model presented encompasses the effects of magnetic activity at all latitudes, effects due to longitude, as well as the variations considered by Fremouw et al. As evaluation of the model's parameters is carried out in terms of irregularities with power law spatial statistics(ref.6) rather than the Gaussian statistics used previously(ref.7), the model is thus applicable to a wide range of transionospheric operating frequencies.

In Section 2 the importance of the use of power law statistics will be considered and the latitude variation of irregularity shape employed in the model will be defined. Section 3 outlines the implementation of Pope's modelling of the high latitude magnetic activity effects, while Section 4 describes how the effects of magnetic activity at low latitude have been included in the model. The incorporation of longitude effects in the model are considered in Section 5. Section 6 outlines the method of modelling the blackout factor which is required in the simulation of spread-F occurrence statistics at the higher latitudes. Section 7 describes checks of the validity of the model with the aid of some independent data bases and the implications and limitations of the model are discussed in Section 8.

2. IRREGULARITY SIZE AND SHAPE

Classically a Gaussian distribution of irregularity size was assumed in scintillation studies(ref.7). The early scintillation observations, which were carried out in the VHF region seemed to be explicable in terms of this type of distribution which appeared to peak at a dominant scale size approximately equal to the radius of the first Fresnel zone for this frequency range, i.e. at about 1km. The reliability of the Gaussian distribution was first thrown into doubt with the unexpected observation of scintillation at gigahertz frequencies near the magnetic equator(refs.8,9). Subsequent in-situ measurements(refs.10,11) and scintillation spectral studies(refs.12,13,14) have shown that the irregularities in the F-region have a power law spectrum involving a wide range of wavenumbers corresponding to dimensions ranging from a few metres to tens of kilometres.

At any observing frequency, the scintillation mechanism is most sensitive to those irregularities whose sizes are the order of the Fresnel dimension(refs.15,7). Hence, while calculations based on the power law spectrum of irregularity size yield similar results to those based on the classical Gaussian distribution at frequencies in the VHF region, the spectral approach allows a more realistic interpretation of the observations in the gigahertz frequency range. For this reason it is important that a model of irregularity behaviour intended for universal application should not only embody a power law irregularity spatial spectrum but, where observations of

scintillation index are used to evaluate its parameters, the associated index calculations should be based on the power law theory. The model outlined in this paper has been constructed in this way.

It is convenient to define(ref.7) the scintillation index S_4 of a fluctuating radio wave (whose amplitude is R) by

$$S_4 = \left[\overline{R^4} - (\overline{R^2})^2 \right]^{\frac{1}{2}} / (\overline{R^2})$$

In this case, it can be shown(ref.6) that, for weak scattering conditions in the irregular ionosphere (i.e. when $\phi_0 < 1$ radian),

$$S_4 = 2^{\frac{1}{2}} \phi_0 F f(\beta) \qquad (1)$$

where

ϕ_0 = r.m.s. phase level of the wave leaving the irregular region,

$$= \left\{ \pi^{\frac{1}{2}} (r_e \lambda) \Delta N (\Delta h \alpha)^{\frac{1}{2}} / 2^{\frac{1}{4}} (\beta k_0)^{\frac{1}{2}} \right\} (\sec\chi)^{\frac{1}{2}} \qquad (2)$$

F = filter function,

$$= \left\{ 1 - \exp(-\mu) \right\}^{\frac{1}{2}}$$

$f(\beta)$ = propagation geometric factor,

$$= (3\beta^4 + 2\beta^2 + 3)^{\frac{1}{2}} / \left\{ 2(2)^{\frac{1}{2}} \right\}$$

$\mu = (\lambda z / 2\pi) k_o^2 = 2k_o^2 / k_f^2$

r_e = classical radius of the electron,

λ = radio wavelength,

Δh = thickness of the irregular layer,

z = mean distance between observer and the irregularities,

α = axial ratio of the field-aligned irregularities,

$\beta^2 = \cos^2\psi + \alpha^2 \sin^2 \psi$

ψ = angle between ray and magnetic field

k_o = outer scale wavenumber of the irregularity spectrum

k_f = Fresnel wavenumber $= (4\pi/\lambda z)^{\frac{1}{2}}$

χ = ray's zenith angle at the ionosphere,

and ΔN = electron density fluctuation.

The derivation of equation (1) is based on a power law irregularity spectrum $P_{\Delta N}(k_r, k_s)$ of the form

$$P_{\Delta N}(k_r, k_s) \propto \left\{ 1+(k_r^2 + k_s^2)/k_o^2 \right\}^{-p/2}$$

where p = the three-dimensional spectral index,
k_s = the wavenumber component along the Earth's magnetic field and
k_r = the wavenumber component radially in a plane normal to the field.

There is ample experimental evidence(refs.12,14) to suggest that p is about 4 and this value has been adopted in the model. Also, while equation (1) applies to the weak scattering case, there is no equivalent strong scattering expression for S_4. Consequently, as in the previous modelling studies(refs.1,2,5), equation (1) is applied universally.

The incidence of scintillation in the gigahertz range in the disturbed equatorial region but not elsewhere implies that the concentration of strong irregularities ($\Delta N/N$ large) of small scale size is higher in this region than elsewhere. This was originally thought to be the result of a low outer scale size (e.g. 100 m) in the irregularity spectrum(refs.16,17) coupled with "normal" values of $\Delta N/N$. More recently, it was pointed out(ref.18) that the gigahertz observations are consistent with the monotonic power law irregularity spectrum normally associated with VHF/UHF scintillation (outer scale size $\approx$ 10 km) because of the large irregularity amplitudes ($\Delta N/N$ approaching 100%) that are often present in the equatorial region(ref,19). This latter view is also consistent with the irregularity wavenumber spectrum of monotonic power-law form between 7 km and 20 m obtained from in-situ observations both in the equatorial region and elsewhere(ref.10,20,21). Consequently, the present model has been constructed on the basis of a wavenumber spectrum of monotonic power-law form involving an outer scale size of 10 km.

The irregularities are believed to be elongated along the Earth's magnetic field. Fremouw and Bates(ref.1) and Fremouw and Rino(ref.2) in their original models assumed a constant value of ten for the elongation factor (a) at all latitudes. This figure is probably justified in the equatorial region where values of a in excess of 7.5 have been observed(ref.22). However, at the high latitudes (50 geomagnetic and above) values of a in the vicinity of 5 have been observed(ref.23). Consequently, in the present model a is represented by

$$a = 10 - 2.5\left[1+\mathrm{erf}\left\{(\theta - 35)/10\right\}\right]$$

which gives $a = 10$ for geomagnetic latitudes (θ) from 0° to 15°, $a = 5$ for 50° < θ <90° and a smooth transition of a from 10 to 5 between 15° and 50° geomagnetic latitude.

3. HIGH LATITUDE MAGNETIC ACTIVITY BEHAVIOUR

Fremouw's original model of global scintillation behaviour(refs.1,2) suffered from the limitation that it took no account of the well established dependence of scintillation occurrence on magnetic activity (e.g. reference 24). By and large this dependence includes a correlation of scintillations with magnetic disturbance which is negative in the equatorial region but which is positive at magnetic latitudes in excess of 50°. The high latitude effect is largely due to the equatorwards movement of the edge of the polar region of high scintillation activity (the scintillation boundary) with increasing magnetic activity(ref.25). Pope(ref.5) modified Fremouw's model so as to

adequately represent the movements of the scintillation boundary caused by changing magnetic activity. Pope's variant of the model will now be outlined.

The model of the incremental electron density (ΔN) in the irregularities consists of four additive terms, the influence of each being dominant in different regions of geomagnetic latitude, namely equatorial, mid, high and auroral latitudes. These terms are functions of some or all of the following parameters: local time (t hours), day of year (D days), geomagnetic latitude (θ degrees), three hourly planetary K magnetic index (Kp) and the monthly smoothed Zurich sunspot number (R). In order to retain the option of adding variations involving other variables into the expression, a factor m has been included in each term which allows the adjustment of its magnitude. Thus the model is represented by

$$\Delta N = m_e \Delta N_e(R,D,t,\theta) + m_m \Delta N_m(t,\theta) + m_h \Delta N_h(Kp,t,\theta) + m_a \Delta N_a(R,t,\theta) \quad (3)$$

where the subscripts e,m,a and h refer to the equatorial, middle, auroral and high latitude regions respectively.

Using units of electrons/m^3 for electron density, the ΔN terms in equation (3) are as follows(refs.2,5)

$$\Delta N_e = 5.5 \times 10^9 (1+0.05R)\left[1-0.4\cos\left\{4\pi(D+10)/365\right\}\right]. \left[\exp\left\{-(t/4)^2\right\} + \exp\left\{-(t-23.5)^2/3.5^2\right\}\right] \exp\left\{-(\theta/\theta_e)^2\right\} \quad (4)$$

$$\Delta N_m = 6 \times 10^8 \left\{1+0.4\cos(\pi t/12)\right\} \exp\left\{-(\theta-\theta_o)^2/\theta_m^2\right\}$$

$$\Delta N_h = 2.7 \times 10^9 \left[1+\mathrm{erf}\left\{(\theta-\theta_b)/\theta_h\right\}\right] \quad (5)$$

$$\Delta N_a = 5.0 \times 10^7 R \exp\left[-\left\{\theta-70+2\cos(\pi t/12)\right\}^2 / \left\{0.03R\right\}^2\right]$$

where

$$\theta_b = 68-\left[0.75+0.25\cos\left\{\pi(t-21)/12\right\}\right]Kp-7.5\cos\left\{\pi(t-21)/12\right\} \quad (6)$$

$$\theta_h = 7 - 3\cos\left\{\pi(t-21)/12\right\} \quad (7)$$

$$\theta_e = 12^\circ, \ \theta_m = 10^\circ \text{ and } \theta_o = 32.5^\circ$$

Singleton(ref.4) noted that the sunspot cycle variation of ΔN implied by spread-F morphology(refs.26,27) is inadequately modelled by the above equations. This position can be rectified however, if the following sunspot number variations of θ_e, θ_m, θ_o, m_e,m_m ,m_h and m_a are incorporated in the model(ref.4).

$$\theta_e = -11.5R+34.5$$

$$\theta_m = 6.75+0.0165R-(3.25-0.0165R)\cos(\pi D/182.5)$$

$$\theta_o = -0.085R+49 \quad (8)$$

$$m_e = -0.011R+3.2 \quad (9)$$

$$m_m = -0.032R+8.6$$

$$m_h = -0.041R+11$$

and $m_a = -0.066R+15$

Note that the polewards shift of the mid-latitude region from the position employed by Fremouw and Rino(ref.2), which was found by Pope(ref.5) to be a necessary adjunct to his modification of the ΔN_h term (equations(5), (6) and (7)), is accommodated by equation(8).

4. LOW LATITUDE MAGNETIC ACITIVITY BEHAVIOUR

Contrary to its effect at high latitudes, at low latitudes increased magnetic activity tends to inhibit the occurrence of both spread-F and scintillation(refs.28,29). The effect is found to be more pronounced at sunspot maximum than at sunspot minimum. The detailed nature of the correlation between scintillation index and magnetic activity was investigated by Koster(ref.30) whose results for Legon are reproduced in figure 1. Here scintillation-index observations, obtained between July and December in a year of high sunspot activity (1969), were first normalised so as to remove the seasonal and diurnal variations and then plotted against the 24 h sum of the appropriate day's Kp indices(S_K). Though there is considerable scatter, the diagram suggests that there is some value of S_K below which scintillation index is independent of S_K and above which scintillation index is decreased with increasing S_K. Koster suggested a Kp sum of 30 as the boundary between these two regimes.

4.1 The model employed

Section 4.2 considers the effect of magnetic activity on spread-F occurrence season by season. There it will be suggested that the Kp sum which separates the regime of constant response from that of inhibition varies with season. In fact, the modelling process is best served by the three lines drawn on figure 1, one for each of the seasons indicated. Each of the lines is accommodated by the scatter and indeed they suggest one plausible reason for the scatter at the higher S_K values. In the present context, the three lines are taken as the variation of scintillation index with magnetic activity. The variation is incorporated in the model by including in m_e (equations (3) and (9)) a factor F_K given by

$$F_K = F_C \qquad 0 < S_K < B_K \qquad (10)$$

$$F_K = F_C - A_K(S_K - B_K) \qquad B_K \leqslant S_K < (B_K + F_C/A_K) \qquad (11)$$

$$F_K = 0 \qquad S_K \geqslant (B_K + F_C/A_K) \qquad (12)$$

where

F_C = constant level of the magnetic factor F_K for the low values of S_K and

A_K = rate of decrease of F_K for S_K greater than its critical value B_K.

The modified model can be tested against some scintillation index data obtained at 45 MHz, at Accra(ref.29). The result of analysing this data to obtain diurnal distributions for both the international magnetically quiet days (circles) and disturbed days (crosses) during sunspot maximum is reproduced in figure 2(a). Unfortunately, the data were not quantified in terms of one of the well-known scintillation indices but rather in terms of a subjective quantity called degree of scintillation. As scintillation is quite severe in the equatorial region, it is not unreasonable to expect the observers to adopt a maximum degree of scintillation figure, namely 5, corresponding to a scintillation index of 1.0. On this basis, it is possible to employ the model, together with the published Kp and sunspot number values, to simulate the degree of scintillation throughout each of the international magnetically quiet and disturbed days during 1957 at Accra. Averaging over all quiet and over all disturbed days gives the diurnal curves shown as full and broken lines respectively in figure 2 (a). The success of the modified model in predicting the overall levels of scintillation activity under magnetic quiet and disturbed conditions is immediately obvious.

Fremouw and Rino(ref.2) employed an equatorial diurnal factor which

(a) peaked at 2330 hours,
(b) fell off exponentially at earlier and later times according to an exponent equal to the square of the time from the maximum, and
(c) involved a time constant of 4 h before and 3.5 h after the time the factor maximizes.

That is, the equatorial diurnal factor which appears in equation (4) is

$$F'_d = \exp\left[-(t/4)^2\right] + \exp\left[-\left\{(t-23.5)/3.5\right\}^2\right]$$

In order to obtain a good fit between the predicted curves and the experimental points on figure 2(a), this diurnal factor had to be modified as follows. The peak was shifted to 2200 hours, the early evening exponential fall-off required a time constant of 3 h and an exponent equal to the fourth power of the time from the peak. On the other hand, the late evening and early morning exponential decay required a time constant of 7 h and an exponent equal to the ninth power of the time from the peak. That is

$$F'_d = \exp\left[-(t/3)^2\right] + \exp\left[-\left\{(t-22)/7\right\}^9\right]$$

Koster and Wright(ref.29) also carried out an analysis using spread-F occurrence data obtained at Ibadan which was similar to that described above for their Accra scintillation data. The resulting diurnal distributions for the quiet days (circles) and disturbed days (crosses) during sunspot maximum (1957) are shown in figure 2(b). In order to use this data to evaluate and improve the ΔN model, it is necessary to employ the following extension of the scintillation model to embrace spread-F occurrence(ref.3).

The spread-F extension of the ΔN model combines the ΔN model with one for the maximum electron density (N) of the F-layer(refs.31,32). It assumes that the spread in critical frequency of the O ray (Δf_o) results from the presence of irregularities at the peak of the height distribution of the F-layer electron density. Consequently

$$\Delta f_o = 8.98 \times 10^{-6} \left\{ (N + \Delta N)^{\frac{1}{2}} - N^{\frac{1}{2}} \right\} \quad (13)$$

where the units of MHz and electrons m^{-3} are used for frequency and electron density respectively.

Since the models provide mean values of the distributions of N and ΔN which might be observed at any location, time, season or epoch of the sunspot cycle, Δf_o is also the mean value of a distribution of possible frequency-spreading events. Assuming that this distribution is normal and involves predominantly positive values of Δf, it can be shown(ref.3) that the percentage occurrence of frequency spreading P_S is given by

$$P_S = 50 \left[1 - \text{erf} \left\{ \sqrt{2} (\Delta f_C / \Delta f_o - 1) \right\} \right] \quad (14)$$

where Δf_C is the minimum spread in critical frequency, which can be detected and which is of the order of 0.1 MHz for a conventional ionosonde(ref.33).

Using equations (13) and (14), together with the ΔN model, it is possible to simulate spread-F percentage occurrence data such as that of Koster and Wright(ref.29) which is presented in figure 2(b). The curves for magnetically quiet and disturbed days resulting from such calculations are shown as full and broken lines respectively in figure 2(b).

As pointed out by Fremouw and Rino(ref.2), the scintillation index modelling process is really a simulation of the product $\Delta N(\Delta h)^{\frac{1}{2}}$, where ΔN is the incremental electron density in the irregularities and Δh is the thickness of the irregular layer. The spread-F extension of the model(ref.3), however, employs only ΔN. Consequently, a diurnal variation in ΔN implied from scintillation data alone may be confused by any diurnal variation in Δh. However, this will not be the case for diurnal variations of ΔN obtained from spread-F data. It has been customary in F-region irregularity modelling to date to use a constant value of Δh, namely 100 km, when considering scintillation data. However, the degree of fit between the model and the spread-F data illustrated in figure 2(b) can only be obtained if the ΔN diurnal variation, based on the scintillation data, is altered to accommodate a Δh, in the equatorial region, which is assumed to vary smoothly during the night from 10 km at 1800 hours to 100 km at 2400 hours and 1000 km at 0600 hours. That is Δh is assumed to vary as

$$\Delta h = 10^{(1+t_{18}/6)} \quad (15)$$

where t_{18} is local time in hours from 1800 LMT. Consequently, the diurnal factor in the equatorial term of the Fremouw and Rino model of ΔN has to be modified so that when combined with this nocturnal variation of Δh, no change is made to $\Delta N(\Delta h)^{\frac{1}{2}}$. This yields the following height corrected diurnal factor

$$F_d = 10 \left(\exp \left[-(t/3)^2 \right] + \exp \left[- \left\{ (t-22)/7 \right\}^9 \right] \right) / 10^{(1+t_{18}/6)/2} \quad (16)$$

In this way, the modelling of scintillation index remains unaltered while allowing a successful modelling of spread-F occurrence.

The postulated increase of Δ h during the night (equation (15)) is consistent with the known behaviour of the F-layer irregularities in the equatorial region. In this region spread-F first appears after sunset well below the layer peak and spreads to the higher reaches of the layer after midnight(refs.34,35). Further evidence indicating the tendency for the irregular region to increase in depth as the night progresses is provided by the Jicamarca radar observations of the irregular equatorial F layer(ref.36). Here it is demonstrated that, as the night progresses, plume-like irregularity structures extending over several hundreds of kilometres of altitude span the layer peak.

4.2 Choice of the seasonal magnetic factors

Returning to the seasonal variation of the process of inhibition of F-layer irregularities with increasing magnetic activity, some experimental spread-F occurrence results due to Lyon, Skinner and Wright(ref.28) will be considered. As shown in figure 3, sunspot maximum data were used to produce diurnal percentage occurrence diagrams for magnetic quiet days (circles) and disturbed days (crosses). In this case, the results average the data obtained at several observing stations in the Afro-Indian zone (20°W to 80°E longitude), while the curves simulated with the modified model are appropriate to Ibadan (3.9°E).

Two changes to the seasonal dependence of the original Fremouw and Rino model were found to be necessary in order to obtain the fit between the simulated diurnal variations and the experimental variations illustrated in figure 3. The first involves adopting the magnetic inhibition relationships already described in Section 4.1, i.e. equations (10), (11) and (12) where F_C is 1.05, B_K is 17 in the southern solstice, 19 in the equinox and 27 the northern solstice and where $(B_K + F_C/A_K)$ is 45. The second modification involves the overall seasonal variation in ΔN. Fremouw and Rino(ref.2) model the seasonal variation as a simple sinusoidal semi-annual variation peaking in the equinoxes (equation (4)). However, as Koster(ref.30) points out, there is also a considerable annual variation in scintillation index as observed at Legon and such a variation has been included in the modified model. Fremouw and Rino's semi-annual variation of amplitude 0.4 was replaced by one of amplitude 0.36 together with an annual variation of amplitude 0.25. That is, the seasonal term in equation (4), namely

$$F_S = \left[1 - 0.4 \cos\left\{ 4\pi(D+10)/365 \right\} \right]$$

was replaced by

$$F_S = \left[1 - 0.36 \cos\left\{ 4\pi(D+10)/365 \right\} + 0.25 \cos\left\{ 2\pi(D+10)/365 \right\} \right] \quad (17)$$

4.3 Sunspot cycle effect

The investigation of scintillation at Accra and spread-F at Ibadan by Koster and Wright(ref.29) besides giving the sunspot maximum results modelled in figure 2, also presents similar results under sunspot minimum conditions (1954). These are illustrated in figure 4 in which the quiet-day results are again depicted by circles and disturbed-day results by crosses. The modified model's predictions for both magnetic quiet and

disturbed conditions (full and broken lines respectively) are also shown. Only two changes are found to be necessary to produce the illustrated degree of fit between the simulation and experiment. The first involves the diurnal distribution factor. Here the peak is shifted from the sunspot maximum value of 2200 hours to 2130 hours. Also, an exponent in the late-evening and early-morning decay, which is equal to the second power of the time from the maximum, is found to be necessary, rather than one involving the ninth power, as at sunspot maximum. That is

$$F_d' = \exp\left[-(t/3)^4\right] + \exp\left[-\left\{(t-21.5)/6\right\}^2\right]$$

The second modification involves the variation of the thickness of the disturbed region throught the night. This is required to vary from 10 to 50 km from 1800 to 0600 hours in sunspot minimum as compared to 10 to 1000 km during this period in sunspot maximum. Hence at sunspot minimum

$$\Delta h = 10^{(1+t_{18}/18)} \tag{18}$$

and the height corrected diurnal factor becomes

$$F_d = 10\left(\exp\left[-(t/3)^4\right] + \exp\left[-\left\{(t-21.5)/6\right\}^2\right]\right)/10^{(1+t_{18}/18)/2} \tag{19}$$

Equations (15) and (18) can be generalized to give

$$\Delta h = 10^{(1+t_{18})}$$

Similarly equations (16) and (19) yield the general form

$$F_d = 10\left(\exp\left[-(t/3)^4\right] + \exp\left[-\left\{(t-t_m)/\tau_m\right\}^q\right]\right)/10^{(1+t_{18}/\tau_{18})/2}$$

and the variation from sunspot maximum to minimum conditions can be accounted for in the model by employing the expressions

$t_m = 21.5 + 0.0025R$

$\tau_m = 6.0 + 0.005R$

$q = 2.0 + 0.035R$

$\tau_{18} = 18-0.06R$

5. THE LONGITUDE DEPENDENCE AT LOW LATITUDE

Lyon, Skinner and Wright(ref.28) analysed spread-F data obtained during the I.G.Y. at fifty-seven equatorial and near equatorial stations. They divided the stations into three geographic longitude zones. The American zone

(longitudes 45° W to 85° W), African zone (longitudes 20° W to 80° E) and the Asian zone (100°E to 160°E) and produced magnetic latitude variations of occurrence, season by season, for each zone. Their data points are reproduced in figure 5. The filled circles represent the observed occurrence situation during magnetically quiet days and the crosses correspondingly for magnetically disturbed days. The curves drawn on figure 5 are not those drawn freehand by Lyon, Skinner and Wright(ref.28) and should be neglected for the moment.

As Lyon, Skinner and Wright point out, the points on figure 5 show that there are longitudinal and seasonal variations in

(a) the overall occurrence of spread F,

(b) the extent of the occurrence reduction accompanying magnetic activity

(c) the width of the equatorial region of enhanced spread-F activity, and

(d) the position of the region with respect to either the magnetic or geographic equator.

The following sections will consider the inclusion of these variations in the irregularity model.

It should be noted that the results for the African zone (figures 5(b),(e) and (h)) were derived from the same data used to produce the duirnal variations of figure 3. As these duirnal variations have been accommodated by the model already (Section 4.2), the model as described above should predict the occurrence levels of the peaks for both quiet and disturbed days in figures 5(b), (e) and (h). This is found to be the case. Of course the model, as it stands, also predicts similar levels for all other longitudes which is obviously erroneous.

5.1 Quiet-day occurrence

The quiet-day occurrence of spread F in the equatorial region (figure 5) not only varies with season and magnetic activity as discussed in Section 4.2, it also varies with longitude. In order to establish a basis on which to model the longitudinal-seasonal variation, the seasonal factor (equation (17)) was replaced in equation (4) by a particular value which will be called a peak occurrence factor. This was done for each of the nine combinations of season and longitude displayed in figure 5. These values were chosen so as to cause the model's prediction of spread-F occurrence to fit the observed quiet day values at the equatorial occurrence peak. These calculations employed the values of Kp and sunspot number observed during the appropriate periods. As expected in the African zone, the peak occurrence factors are as given by equation (17).

The points shown as filled circles, squares and triangles (without the connecting lines) in figure 6(a) give the peak occurrence factor plotted against the day of year for each longitude zone. In figure 6(b) the peak occurrence factors are plotted in similar fashion against geomagnetic longitude for each season. The modelling process now requires mathematical expressions to be developed which will describe the variations of the peak occurrence factor with day of year and longitude.

Examination of each of the three families of points in figure 6(a) suggests that a semi-annual plus annual variation such as that suggested in Section 4.2 (equation (17)) should adequately describe the seasonal variations. Indeed equation (17) describes the form of the African zone (Ω=70°) variation.

Unfortunately the situation is not so clear cut in the case of the longitudinal variations (figure 6(b)). The lack of information between

200° and 360° geomagnetic longitude makes it difficult to model the longitudinal variation unambiguously.

A simple sine curve could be fitted to the data points. When this is done the curve is found to go negative over some 100° of longitude. This intolerable situation could be overcome by assuming the peak occurrence factor is zero or some small value in this longitude range. Such a model would predict zero or light spread-F and scintillation occurrence in the mid-Pacific area. However, as this is inconsistent with the sketchy information available in this area(ref.37,38), this mathematical form was rejected.

The longitude variation adopted involved a two peak variation of the peak occurrence factor (F_S) given by

$$F_S = p\left\{1 + S\cos\Omega - H\cos(2\Omega)\right\} \tag{20}$$

The seasonal variation can be adequately included if the coefficients in equation (20) are given by

$$P = EP\left[1-AP\cos\left\{2\pi(D+10)/365\right\} - SP\cos\left\{4\pi(D+10)/365\right\}\right] \tag{21}$$

$$S = ES\left[1-AS\cos\left\{2\pi(D+10)/365\right\} - SS\cos\left\{4\pi(D+10)/365\right\}\right] \tag{22}$$

$$H = EH\left[1-AH\cos\left\{2\pi(D+10)/365\right\} - SH\cos\left\{4\pi(D+10)/365\right\}\right] \tag{23}$$

Equations (20) to (23) inclusive generate a surface in the factor, day of year, geomagnetic longitude three dimensional space. This surface fits the experimental points and has the factor versus day of year and the factor versus geomagnetic longitude cross-sections shown by the curves in figures 6(a) and (b) respectively, when

EP = 0.628, AP = -0.0170, SP = 0.402

ES = -0.08, AS = 1.375, SS = 1.25

EH = 0.5, AH = -0.08, SH = -0.06

The implications of this and the other longitude variations chosen will be considered further in Sections 7 and 8.

5.2 Critical value of Kp sum

From figure 5 it is obvious that the extent of the reduction in spread-F occurrence accompanying increased magnetic activity varies with both season and longitude. In Section 4.1 it was suggested that the occurrence reduction occurs when the 24-hour Kp sum surpasses some critical value. Variation of this critical value with season and longitude therefore, provides the basis for a model of the magnetic activity effect. As explained for the case of the peak occurrence factor (Section 5.1), the critical Kp sum for each of the combinations of longitude and season represented in figure 5 can be determined by forcing the model to reproduce the disturbed day peak occurrences shown in figure 5. The required values of the critical Kp sums (B_K) are plotted against day of year and geomagnetic longitude as the points shown as filled circles, squares and triangles (without the connecting lines) on figures 6(c) and

(d). The points for the geomagnetic longitude of 70° in both these diagrams are as obtained previously for this longitude (Section 4.2).

As described in the previous section for the peak occurrence factor, a set of mathematical expressions are needed to represent the seasonal and latitudinal variations implied by the points in figures 6(c) and (d). The disposition of the points in figure 6(d) suggests that, in this case, a simple sine function might be more appropriate than the double peaked longitude function employed for the peak-occurrence factor. The annual plus semi-annual seasonal function used for the peak-occurrence factor also appears to be appropriate here. Thus the set of equations employed are as follows:

$$B_K = K\left[1 - AK\cos\left\{2\pi(D+10)/365\right\} - SK\cos\left\{4\pi(D+10)/365\right\}\right] \quad (24)$$

where

$$K = CK\left\{1 + EK\cos(\Omega + \psi_K)\right\} \quad (25)$$

$$AK = CAK\left\{1 + BAK\cos(\Omega + \psi_{AK})\right\} \quad (26)$$

and

$$SK = CSK\left\{1 + BSK\cos(\Omega + \psi_{SK})\right\} \quad (27)$$

Equations(25) to (27) can be written more conveniently as:

$$K = KA + KE\cos\Omega + KC\sin\Omega \quad (28)$$

$$AK = (AKA + AKE\cos\Omega + AKC\sin\Omega)/K \quad (29)$$

$$SK = (SKA + SKB\cos\Omega + SKC\sin\Omega)K^{-1} \quad (30)$$

Equations (24) and (28) to (30) inclusive generate a surface in the critical Kp sum, day of year, geomagnetic longitude three dimensional space. This surface fits the experimental points and has the critical Kp sum versus day of year and critical Kp sum versus geomagnetic longitude cross sections shown by the curves in figures 6(c) and (d) when

KA = 24.61, KB = 6.88, KC = -6.89

AKA = -1.09, AKB = 2.09, AKC = 5.72

SKA = 22.57, SKB = 8.43, SKC = -6.87

5.3 Incremental width

Fremouw's original model of ΔN assumed that the equatorial region of high activity was centred on the geomagnetic equator and fell off with

latitude according to $\exp\left\{-(\theta/\theta_e)^2\right\}$ where θ_e is a constant "width" of 12°. Examination of figure 5 suggests this is an approximation with regard to both the position of the peak and its width. While the question of width will be examined in this section and that of peak position in the next section, in practice the modelling procedures involved were necessarily carried out in concert.

A value of θ_e was found which, when substituted for θ_e in equation (4) allowed the model (equation(3)) to adequately represent the spread-F data for each of the seasons and longitudes represented in figure 5. The corresponding incremental widths ($\Delta\theta_e = \theta'_e - \theta_e$) are plotted against day of year and geomagnetic longitude as the points shown as the filled circles, squares and triangles (without the lines) on figures 6(e) and (f). A group of equations, similar to those used in the previous section, were found which adequately model the distributions of points in figures 6(e) and (f). These yield the curves shown in the figures and are

$$\Delta\theta_e = T\left[1 - AT\cos\left\{2\pi(D+10)/365\right\} - ST\cos\left\{4\pi(D+10)/365\right\}\right]$$

$$T = TA + TB\cos\Omega + TC\sin\Omega$$

$$AT = (ATA + ATB\cos\Omega + ATC\sin\Omega)/T$$

$$ST = (STA + STB\cos\Omega + STC\sin\Omega)/T - 1$$

where

TA = 4.86,	TB = 3.14,	TC = -0.994
ATA = 1.98,	ATB = -0.98,	ATC = -1.75
STA = 6.16,	STB = 6.84,	STC = -3.72

5.4 Latitude of the occurrence peak

As indicated in Section 5.3, the peak of irregularity activity in the equatorial region is not always on the geomagnetic equator and the model should allow for the deviations. This, together with the variations in width just discussed, is taken into account by replacing the $\exp\left\{-(\theta/\theta_e)^2\right\}$ term in equation (4) by $\exp\left[-\left\{(\theta+\theta_d)/(\theta_e+\Delta\theta_e)\right\}^2\right]$. Using the techniques described in the previous three sections, the deviations can be found for each of the seasons and longitudes represented in figure 5. These are plotted against day of year and geomagnetic longitude as the points (filled circles, squares and triangles) on figures 6(g) and (h). A set of equations can then be found which will model these variations in θ_d and yield the lines drawn on figures 6(g) and (h). The resulting expressions are

$$\theta_d = V\left[1 - AV\cos\left\{2\pi(D+10)/365\right\} - SV\cos\left\{4\pi(D+10)/365\right\}\right]$$

$$V = VA + VB\cos\Omega + VC\sin\Omega$$

$$AV = (AVA + AVB\cos\Omega + AVC\sin\Omega)/V$$

$$SV = (SVA + SVB\cos\Omega + SVC\sin\Omega)/V-1$$

where

$$VA = -0.508, \quad VB = -1.74, \quad VC = 3.30$$

$$AVA = -2.721, \quad AVB = -5.78, \quad AVC = 5.0$$

$$SVA = -0.873, \quad SVB = -1.13, \quad SVC = 3.47$$

5.5 Total longitude dependence

When the four longitude variations discussed above are included in the model, which is also supplied with the observed values of Kp and sunspot number, the resulting latitude distributions for each of the seasons and longitudes of figure 5 are as shown by the curves on that figure. The full-line curves represent the quiet day situation, while the broken lines are for disturbed days. As expected, the model provides a good simulation of the experimental situation.

Further confidence in the model can be obtained by comparing its predictions with experimental latitude versus local time contour diagrams of spread-F occurrence(ref.28). The full-line contours on figure 7 give the experimental results for each of the seasons and quiet and disturbed days in the African zone. The broken-line contours give the model's predictions. Figure 8 allows a similar comparison to be made for the American zone. The experimental data employed in the production of figures 7 and 8 is the same as that used for figure 5. These successful comparisons indicate therefore, that the latitude, longitude, seasonal and Kp variations modelled with the aid of figure 5 are apparently valid independent of the diurnal variation. Further tests of the validity of the model will be discussed in Section 7.

6. BLACKOUT FACTOR

At latitudes in excess of a critical value θ_C (about 70° geomagnetic), the adaption of the ΔN model to simulate spread-F occurrence (described in Section 4.1, equations (13) and (14)) requires the inclusion of a blackout factor(ref.3). This factor, which is applied directly to the occurrence probability predicted by equation (14), is believed to be due predominantly to the effect of polar blackout on an ionosonde's ability to detect spread-F. The general form of the blackout factor (B) is as follows:

$$B = \left(1+A\left[\cos\left\{2\pi(t-\tau)/24\right\}-1\right]+C\left[\cos\left\{4\pi(t-\tau)/24\right\}-1\right)\right. \cdot \exp\left\{-(\theta-\theta_C)^2/\theta_p^2\right\} \qquad (31)$$

Here the two coefficients A and C together with the epoch τ, critical latitude θ_C and latitudinal decay parameter θ_p are known to vary with season, i.e. D, and sunspot number R(ref.4).

Using the modelling techniques described in Section 5 and data on A, C, τ, θ_C and θ_p given in Singleton(ref.4), it is possible to develop a blackout model

on the basis of equation (31) where

$$A = (0.14-0.000275R)\left[1-(0.7857-0.000987R)\cos\left\{2\pi(D+10)/365\right\}-(0.2149-0.000777R)\cos\left\{4\pi(D+10)/365\right\}\right] \quad (32)$$

$$C = (0.025+0.0003R)\left[1+(2-0.01R)\cos\left\{2\pi(D+10)/365\right\}+(1-0.01R)\cos\left\{4\pi(D+10)/365\right\}\right] \quad (33)$$

$$\tau = (2.75+0.005R)\left[1+0.0073R\cos\left\{2\pi(D+10)/365\right\}+(0.091+0.0032R)\cos\left\{4\pi(D+10)/365\right\}\right] \quad (34)$$

$$\theta_C = (66.25-0.0063R)\left[1+(0.0377-0.0096R)\cos\left\{2\pi(D+10)/365\right\}+(0.0189-0.00048R)\cos\left\{4\pi(D+10)/365\right\}\right] \quad (35)$$

and

$$\theta_p = (229.5+0.019R)\left[1+(0.6144-0.00021R)\cos\left\{2\pi(D+10)/365\right\}-(0.3072-0.00011R)\cos\left\{4\pi(D+10)/365\right\}\right] \quad (36)$$

Equations (32) to (36) inclusive coupled with equations(13) and (14) allow the ΔN model to be converted to a spread-F model applicable at all latitudes.

7. TESTS OF THE MODEL'S VALIDITY

Having developed the model considerably from the initial attempts of Fremouw and Bates(ref.1) and Fremouw and Rino(ref.2) by incorporating information from a number of published data bases, it is of interest to attempt to test the model's validity against other independent data bases. The major changes to the original model initiated in this paper involve the equatorial region and consequently the checks to be described involve this region.

7.1 The longitude variation

Besides the study of equatorial spread F by Lyon, Skinner and Wright(ref.28) used in the formulation of the model, it is difficult to find suitable direct observations of scintillation or spread F against which to check the adopted longitude variation. However, there does exist a significant indirect observation of the longitude variation of scintillation activity which can be simulated. In a study of in-situ measurements of equatorial F-region irregularities Basu, Basu and Khan(ref.19) deduce, from their OGO-6 retarding potential analyser data, a magnetic latitude versus geographic longitude contour map of the percentage occurrence of scintillation activity. The deductions are based on the scintillations $\geqslant$ 4.5 dB expected from the data at 140 MHz between

1900 and 2300 LMT during the period November and December 1969 and 1970 when Ap $\leq$12. The contour map shown in figure 9(b) is obtained when the present model is used to simulate their result which is reproduced in figure 9(a). The simulation is a detailed one in that the statistics are obtained from scintillation index values calculated from the model for each half hour throughout the period, taking the observed values of Kp and sunspot number into account.

Comparison of figures 9(a) and (b) shows that the model reproduces the main features of the experimental (though indirect) longitude distribution. A discrepancy involves the magnitude of the secondary occurrence peak at about 170° W; the model suggests this rises to 80% while the observations imply a 40% occurrence. It will be recalled that the lack of observations in this longitude range in the Lyon, Skinner and Wright(ref.28) study, made choice of a mathematical description for the longitude variation difficult (Section 5.1). The observations of Basu, Basu and Khan(ref.19) suggest that while a double peaked longitude distribution is appropriate, the peaks, rather than being of equal magnitude, should involve one over the mid-Pacific area which is smaller than that over Africa. This point will be considered further in Section 8.

7.2 The temporal and magnetic variations

The model put forward here differs from that of Fremouw and Rino(ref.2) in the equatorial region, not only in terms of variations associated with longitude but also in terms of diurnal, seasonal, sunspot-cycle and magnetic activity variations. To test the model's ability to deal with these latter variations some spread-F data reported by Cole and McNamara(ref.39) have been simulated. Figure 10(a) reproduces their spread-F occurrence data for Vanimo (2.7°S, 141.3°E, 11°S magnetic), while figure 10(b) presents the simulation. It should be noted that the simulation is a detailed one. The spread-F probability is calculated from the model for each half hour of each day, taking the observed values of Kp and sunspot number into account. These data are then used to compute the diurnal and seasonal variations in the usual way.

Comparison of figures 10(a) and (b) shows that the experimental diurnal and seasonal distributions are well predicted by the model. In years where the equinoctial peak is higher and more persistent throughout the night at one equinox than at the other, the model makes a corresponding prediction. This suggests that the modelled magnetic variation is functioning correctly as this is the variation most likely to be operative in this regard. However, the sunspot cycle variation is not as faithfully modelled. The period examined spans a peak of the sunspot cycle. At the peak (1967-1970), the levels are accurately predicted. However, as the sunspot number decreases in 1971 and 1972, the predicted levels of occurrence fall off more slowly than the experimental levels. Possible reasons for this are discussed in Section 8.

8. DISCUSSION AND CONCLUSIONS

A number of modifications to Fremouw's model of F-layer irregularity strength have been proposed in order to force the model into agreement with a considerable body of scintillation and spread-F data. Particular attention has been paid to the equatorial region where the original model was particularly lacking. However, the original model also has been updated in the other latitude regions in accordance with the findings of other studies. A concise statement of the proposed model, which is thus generally applicable, is given in the Appendix I.

In Section 7.1 reference was made to the discrepancy between the magnitudes of the predicted and observed occurrence peaks at 170° W as indicated in figure

9. The double peaked distribution adopted (equation(20)) in Section 5.1 with two peaks of equal magnitude may require modification. However, the lack of observational information in one of the longitude regions involved, namely the mid-Pacific region, mitigates against improving the model in this respect. Since the indirect scintillation data of Basu, Basu and Khan(ref.19) applies only to southern solstice and sunspot maximum conditions, it does not provide sufficient information at this time to justify changing the model adopted. The exact form of the longitude variation and its changes with season and sunspot cycle, if any, represent the biggest single uncertainty in the proposed model. More observational information in the Pacific equatorial region will be required to resolve this uncertainity.

It is interesting to note in passing that the two peaks occur at the longitudes where the magnetic equator crosses the geographic equator. This suggests perhaps, that these are two influences bearing on the occurrence of the irregularities, one associated with each of the equators and that these influences reinforce where the equators cross. If this is the case, it will not be surprising if the resulting peaks have different natures because of the different configurations of the two equators at the two crossing points. Over the Pacific the equators approach each other gradually over a much larger longitude range than is the case over the Atlantic.

Another area where the proposed model may require refinement is suggested in Section 7.2. The comparison of figures 10(a) and (b) indicates that the detailed predictions of the model may be lacking as the sunspot cycle moves away from its peak. It will be recalled that the model relies heavily on the I.G.Y. observations of Lyon, Skinner and Wright(ref.28) and, as these are for sunspot maximum conditions, this finding is perhaps not surprising. Another factor which must be borne in mind here is that Vanimo, at 11° S magnetic latitude, is on the edge of the equatorial region of high activity and hence will be very sensitive to the variations of the equatorial region's width and centre position which were both modelled with the aid of the I.G.Y. data. The other successful simulations obtained away from the sunspot maximum (e.g. figure 4) attest to the general reliability of the model in the equatorial region throughout the sunspot cycle. Again this question of detail will only be resolved with the aid of more experimental data.

Regardless of these weaknesses, the model is a vast improvement on that originally put forward by Fremouw and Bates(ref.1) and Fremouw and Rino(ref.2). The proposed improvements to the model, not only enhance its usefulness as a simulation technique in engineering studies of propagation configurations affected by F-region irregularities, but should also provide impetus to the understanding of the physics of the irregularities. This is especially true of the areas of magnetic activity control, irregularity layer thickness, and the duirnal, seasonal, longitudinal and sunspot cycle variations of irregularity occurrence and strength.

REFERENCES

No.	Author	Title
1	Fremouw, E.J., and Bates, J.F.	"Worldwide Behaviour of Average VHF-UHF Scintillation" Radio Sci., Vol. 6, p.863, 1971
2	Fremouw, E.J., and Rino, C.L.	"An Empirical Model for Average F-Layer Scintillation at UHF-UHF" Radio Sci., Vol. 8, p.213, 1973
3	Singleton, D.G.	"An Empirical Model of Global Spread-F Occurrence" J. Atmos. Terr. Phys., Vol. 37, p.1535, 1975
4	Singleton, D.G.	"The Reconciliation of an F-Region Irregularity Model with Sunspot Cycle Variations in Spread-F Occurrence" Radio Sci., Vol. 12, p.107, 1977
5	Pope, J.H.	"High Latitude Ionospheric Irregularity Model" Radio Sci., Vol. 9, p.675, 1974
6	Rufenach, C.L.	"Ionospheric Scintillation by a Random Phase Screen: Spectral Approach" Radio Sci., Vol. 10, p.155, 1975
7.	Briggs, B.H., and Parkin, J.A.	"On the Variation of Radio Star and Satellite Scintillation with Zenith Angle" J. Atmos. Terr. Phys., Vol. 25, p.339, 1963
8	Craft, H.D., and Westerlund, L.H.	"Scintillation at 4 and 6 GHz Caused by the Ionosphere" AIAA Paper No. 2 - 179, American Institute of Aeronautics and Astronautics Library, 150 Third Ave., New York, 1972
9	Taur, R.R.	"Ionospheric Scintillation at 4 and 6 GHz" Comsat Tech. Rev., Vol. 3, p.145, 1973
10	Dyson, P.L., McClure, J.P., and Hanson, W.B.	"In-Situ Measurements of the Spectral Characteristics of F-Region Ionospheric Irregularities" J. Geophys. Res., Vol. 79, p.1495, 1974
11	Phelps, A.D.R., and Sagalyn, R.C.	"Plasma Density Irregularities in the High-Latitude Topside Ionosphere" J. Geophys. Res., Vol. 81, p.515, 1976
12	Rufenach, C.L.	"Power-Law Wavenumber Spectrum Deduced from Ionospheric Scintillation Observations" J. Geophys. Res., Vol. 77, p.4761, 1972

No.	Author	Title
13	Rufenach, C.L.	"Wavelength Dependence of Radio Scintillation: Ionosphere and Interplanetary Irregularities" J. Geophys. Res., Vol. 79, p.1562, 1974
14	Singleton, D.G.	"Power Spectra of Ionospheric Scintillation" J. Atmos. Terr. Phys., Vol. 36, p.113, 1974
15	Ratcliffe, J.A.	"Some Aspects of Diffraction Theory and Their Application to the Ionosphere" Ref. Prog. Phys., Vol. 19, p.188, 1956
16	Wernik, A.W., and Liu, C.H.	"Ionospheric Irregularities Causing Scintillation of GHz Frequency Radio Signals" J. Atmos. Terr. Phys., Vol. 36, p.871, 1974
17	Yeh, K.C., Liu, C.H., and Youakin, M.G.	"A Theoretical Study of Ionosphere Scintillation Behaviour Caused by Multiple Scattering" Radio Sci., Vol. 10, p.97, 1975
18	Basu, Sunanda and Basu, S.	"Correlated Measurements of Scintilations and In-Situ F-Region Irregularities from OGO-6" Geophys. Res. Letters, Vol. 3, p.681, 1976
19	Basu, Sunanda, Basu, S., and Khan, B.K.	"Model of Equatorial Scintillations from In-Situ Measurements" Radio Sci., Vol. 11, p.821, 1976
20	Kelly, M.C., and Mozen, F.C.	"A Review of the Recent Results of In-Situ Ionospheric Irregularity Measurements and their Relation to Elestrostatic Instabilities" Proc. Symposium on the Effect of the Ionosphere on Space Systems and Communications, Editor: J.M. Goodman, Naval Research Lab., Washington, D.C., 1975
21	Morse, F.A., Edgar, B.C., Koons, H.C., Rice, C.J., Heikkila, D.J., Hoffman, J.H., Tinsley, B.A., Winningham, J.D., Christensen, A.B., Woodman, R.J., Pomalaza, J., and Teisxeira, W.R.	"EQUION, an Equatorial Ionospheric Irregularity Experiment" Report SAMSC-TR-76-158, Aerospace Corporation, El Segundo, California, 1976

No.	Author	Title
22	Koster, J.R.	"Some Measurements of the Irregularities Giving Rise to Radio Star Scintillations at the Equator" J. Geophys. Res., Vol. 68, p.2579, 1963
23	Singleton, D.G.	"The Dependence of High-Latitude Ionospheric Scintillations on Zenith Angle and Azimuth" J. Atmos. Terr. Phys., Vol. 35, p.2253, 1973
24	Getmantsev, G.G., and Eroukhimov, L.M.	"Radio Star and Satellite Scintillations" Annals IQSY. Vol. 5, p.229, 1969
25	Aarons, J.	"A Descriptive Model of F-Layer High Latitude Irregularities as shown by Scintillation Observations" J. Geophys. Res., Vol. 78, p.7441, 1973
26	Singleton, D.G.	"The Geomorphology of Spread-F" J. Geophys. Res., Vol. 65, p.3615, 1960
27	Singleton, D.G.	"The Morphology of Spread-F Occurrence Over Half a Sunspot Cycle" J. Geophys. Res., Vol. 73, p.295, 1968
28	Lyon, A.J., Skinner, M.J., and Wright, R.W.H.	"The Belt of Equatorial Spread-F" J. Atmos. Terr. Phys., Vol. 19, p.145, 1960
29	Koster, J.R., and Wright, R.W.	"Scintillation, Spread-F and Transequatorial Scatter" J. Geophys. Res., Vol. 65, p.2303, 1960
30	Koster, J.R.	"Equatorial Scintillation" Planet. Space Sci., Vol. 20, p.1999, 1972
31	Ching, B.K., and Chiu, G.J.	"A Phenomenological Model of Global Ionospheric Electron Density in the E-,F1- and F2-regions" J. Atmos. Terr. Phys., Vol. 35, p.1615, 1973
32	Chiu, G.J.	"An Improved Phenomenological Model of Ionospheric Density" J. Atmos. Terr. Phys., Vol. 37, p.1563, 1975
33	Singleton, D.G.	"A Study of Spread-F Ionospheric Echoes at Night at Brisbane. III Frequency Spreading" Aust. J. Phys., Vol. 10, p.60, 1957
34	Haung, Chun-Ming	"F-Region Irregularities that Cause Scintillation and Spread-F at Low Latitude" J. Geophys. Res., Vol. 75, p.4833, 1970

No.	Author	Title
35	Davis, R.M.	"The Occurrence of Spread-F and its Effect on HF Propagation" Telecommunications Res. and Eng. Report No. 28, Institute for Telecom. Science, US Dept. of Commerce, 1972
36	Woodman, R.F., and La Hoz, C.	"Radar Observations of F-Region Equatorial Irregularities" J. Geophys. Res., Vol. 81, p.5447, 1976
37	Reber, G.	"Spread-F over Hawaii" J. Geophys. Res., Vol. 59, p.257, 1954
38	Reber, G.	"World-Wide Spread-F" J. Geophys. Res., Vol. 61, p.157, 1956
39	Cole, D.G., and McNamara, L.F.	"Deviations of Spread-F Occurrence Rates at Near-Equatorial Stations in the Australian Zone" Aust. J. Phys., Vol. 27, p.249, 1974

APPENDIX I

THE PROPOSED MODEL

The following is a concise statement of the scintillation index and spread-F versions of the model which result from the present investigation.

The scintillation index S_4 is given by

$$S_4 = 2^{\frac{1}{2}}\phi_o F f(\beta)$$

where

$$\phi_o = \left[\pi^{\frac{1}{2}}(r_e\lambda)\Delta N(\Delta h\alpha)^{\frac{1}{2}}/2^{\frac{1}{4}}(\beta k_o)^{\frac{1}{2}}\right]\sec\chi)^{\frac{1}{2}}$$

$$F = \left\{1-\exp(-\mu)\right\}^{\frac{1}{2}}$$

$$f(\beta) = (3\beta^4 + 2\beta^2 + 3)^{\frac{1}{2}}/\left\{2(2)^{\frac{1}{2}}\right\}$$

$$\mu = (\lambda z/2\pi)k_o^2$$

$$\beta^2 = \cos^2\psi + \alpha^2\sin^2\psi$$

The probability of occurrence of spread-F is given by

$$P_S = 50B\left[1-\mathrm{erf}\left\{\sqrt{2}(\Delta f_c/\Delta f_o - 1)\right\}\right]$$

where

$$\Delta f_o = 8.98\times10^{-6}\left\{(N + \Delta N)^{\frac{1}{2}} - N^{\frac{1}{2}}\right\}$$

The parametric variations which constitute the models are as follows:

The elongation factor α is given by

$$\alpha = 10-2.5\left[1 + \mathrm{erf}\left\{(\theta-35)/10\right\}\right]$$

The effective thickness Δh is given by

$$\Delta h = 10^{(1+t_{18}/\tau_{18})}$$

The blackout factor B is given by

$$B = \left(1 + A\left[\cos\left\{2\pi(t-\tau)/24\right\} - 1\right] + C\left[\cos\left\{4\pi(t-\tau)/24\right\}-1\right]\right)\exp\left\{-(\theta-\theta_c)^2/\theta_p^2\right\}$$

where

$$A = (0.14-0.000275R)\left[1-(0.7857-0.000987R)\cos\left\{2\pi(D+10)/365\right\} -(0.2143-0.000777R)\cos\left\{4\pi(D+10)/365\right\}\right]$$

$$C = (0.025+0.0003R)\left[1+(2-0.01R)\cos\left\{2\pi(D+10)/365\right\} +(1-0.01R)\cos\left\{4\pi(D+10)/365\right\}\right]$$

$$\tau = (2.75+0.005R)\left[1+0.0073R\cos\left\{2\pi(D+10)/365\right\} +(0.091+0.0032R)\cos\left\{4\pi(D+10)/365\right\}\right]$$

$$\theta_C = (66.25-0.0063R)\left[1+(0.0377-0.0096R)\cos\left\{2\pi(D+10)/365\right\}\right.$$
$$\left.+(0.0189-0.00048R)\cos\left\{4\pi(D+10)/365\right\}\right]$$
$$\theta_p = (229.5+0.019R)\left[1+(0.6144-0.00021R)\cos\left\{2\pi(D+10)/365\right\}\right.$$
$$\left.-(0.307-0.00011R)\cos\left\{4\pi(D+10)/365\right\}\right]$$

The F-layer peak electron density N is given by a model due to Chiu (ref.32) and the incremental electron density in the irregularities ΔN is given by:

$$\Delta N = m_e\Delta N_e(R,D,t,\theta,\Omega,S_K)+m_m\Delta N_m(t,\theta)$$
$$+m_h\Delta N_h(t,Kp,\theta)+m_a\Delta N_a(t,R,\theta)$$

where

$$m_e = 3.2 - 0.011R$$
$$m_m = 8.6 - 0.032R$$
$$m_h = 11.0 - 0.041R$$
$$m_a = 15.0 - 0.066R$$
$$\Delta N_e = 5.5\times10^9 F_d F_s F_K(1+0.05R)\exp\left\{-(\theta+\theta_d)^2/(\theta_e+\Delta\theta_e)^2\right\}$$
$$\Delta N_m = 6.0\times10^8\left\{1+0.4\cos(\pi t/12)\right\}\exp\left\{-(\theta-\theta_o)^2/\theta_m^2\right\}$$
$$\Delta N_h = 2.7\times10^9\left[1+\mathrm{erf}\left\{(\theta-\theta_b)/\theta_h\right\}\right]$$
$$\Delta N_a = 5.0\times10^7 R\exp\left[-\left\{\theta-70+2\cos(\pi t/12)\right\}^2/\left\{0.03R\right\}^2\right]$$
$$F_d = 10\left(\exp\left[-(t/3)^4\right]+\exp\left[-\left\{(t-t_m)/\tau_m\right\}^{\vec{q}}\right]\right)/10^{(1+t_{18}/\tau_{18})/2}$$
$$F_S = P\left\{1 + S\cos\Omega - H\cos(2\Omega)\right\}$$
$$F_K = F_C \qquad \text{for } 0<S_K<B_K$$
$$= F_C - A_K(S_K-B_K) \qquad \text{for } B_K\ll S_K<(B_K+F_C/A_K)$$
$$= 0 \qquad \text{for } S_K\gg(B_K+F_C/A_K)$$
$$\theta_d = V\left[1-AV\cos\left\{2\pi(D+10)/365\right\}-SV\cos\left\{4\pi(D+10)/365\right\}\right]$$
$$\theta_e = -11.5R + 34.5$$
$$\Delta\theta_e = T\left[1-AT\cos\left\{2\pi(D+10)/365\right\}\ ST\cos\left\{4\pi(D+10)/365\right\}\right]$$
$$\theta_o = -0.085R + 49$$
$$\theta_m = 6.75 + 0.0165R-(3.25-0.0165R)\cos(2\pi D/365)$$
$$\theta_b = 68-\left[0.75+0.25\cos\left\{\pi(t-21)/12\right\}\right]Kp-7.5\cos\left\{\pi(t-21)/12\right\}$$
$$\theta_h = 7 - 3\cos\left\{\pi(t-21)/12\right\}$$
$$t_m = 21.5 +0.0025R$$
$$\tau_m = 6.0 + 0.005R$$

$$q = 2.0 + 0.035R$$

$$\tau_{18} = 18.0 + 0.06R$$

$$P = 0.628\left[1+0.170\cos\left\{2\pi(D+10)/365\right\}-0.402\cos\left\{4\pi(D+10)/365\right\}\right]$$

$$S = -0.08\left[1-1.375\cos\left\{2\pi(D+10)/365\right\}-1.25\cos\left\{4\pi(D+10)/365\right\}\right]$$

$$H = 0.5\left[1+0.08\cos\left\{2\pi(D+10)/365\right\}+0.06\cos\left\{4\pi(D+10)/365\right\}\right]$$

$$B_K = K\left[1-AK\cos\left\{2\pi(D+10)/365\right\}-SK\cos\left\{4\pi(D+10)/365\right\}\right]$$

$$V = -0.508-1.74\cos\Omega+3.30\sin\Omega$$

$$SV = (-0.873-1.13\cos\Omega+3.47\sin\Omega)/V-1$$

$$AV = (-2.721-5.78\cos\Omega+5.0\ \sin\Omega)/V$$

$$T = 4.86+3.14\cos\Omega-0.994\sin\Omega$$

$$ST = (6.16+6.84\cos\Omega-3.72\sin\Omega)/T-1$$

$$AT = (1.98-0.98\cos\Omega-1.75\sin\Omega)/T$$

$$K = 24.61+6.88\cos\Omega-6.89\sin\Omega$$

$$SK = (22.57+8.43\cos\Omega-6.87\sin\Omega)/K-1$$

$$AK = (-1.09+2.09\cos\Omega+5.72\sin\Omega)/K$$

Definitions of quantities not specified in the above can be found in the main text.

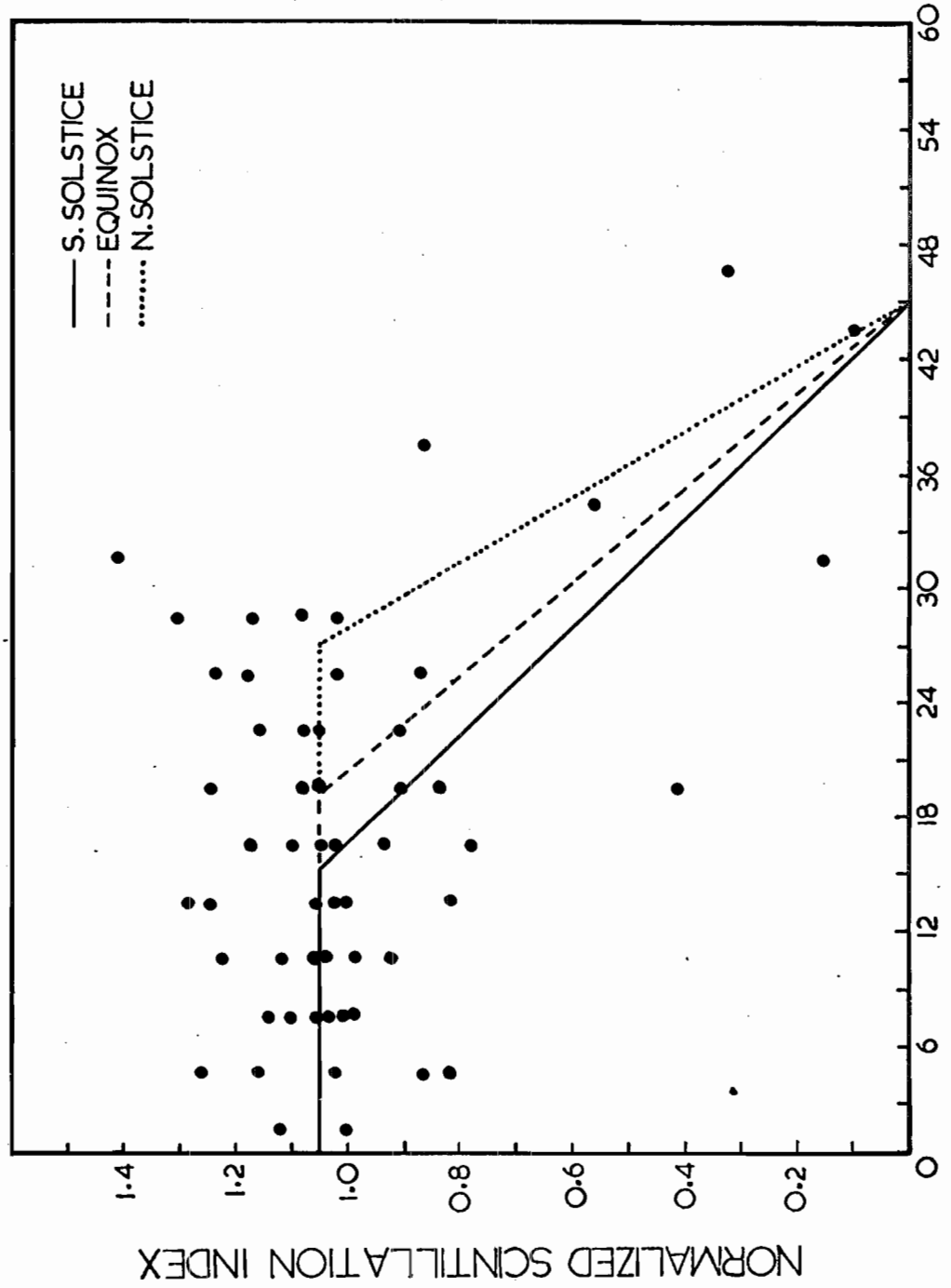

Figure 1. Normalized scintillation index as a function of Kp sum.

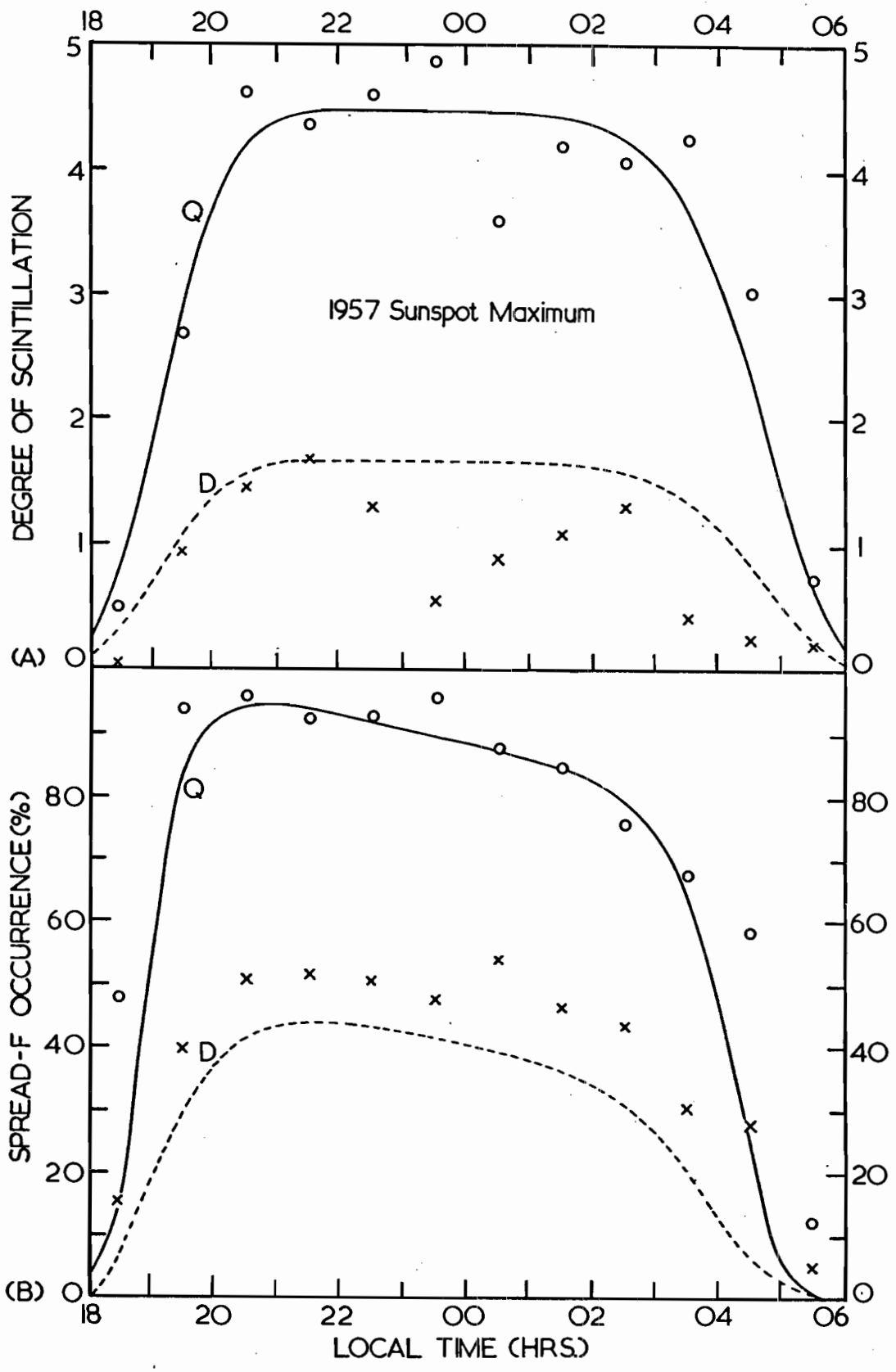

Figure 2. Magnetically quiet and disturbed levels (circles and crosses respectively) of scintillation observed at Accra and spread-F occurrence at Ibadan under sunspot maximum conditions. The curves illustrate the modelled distributions.

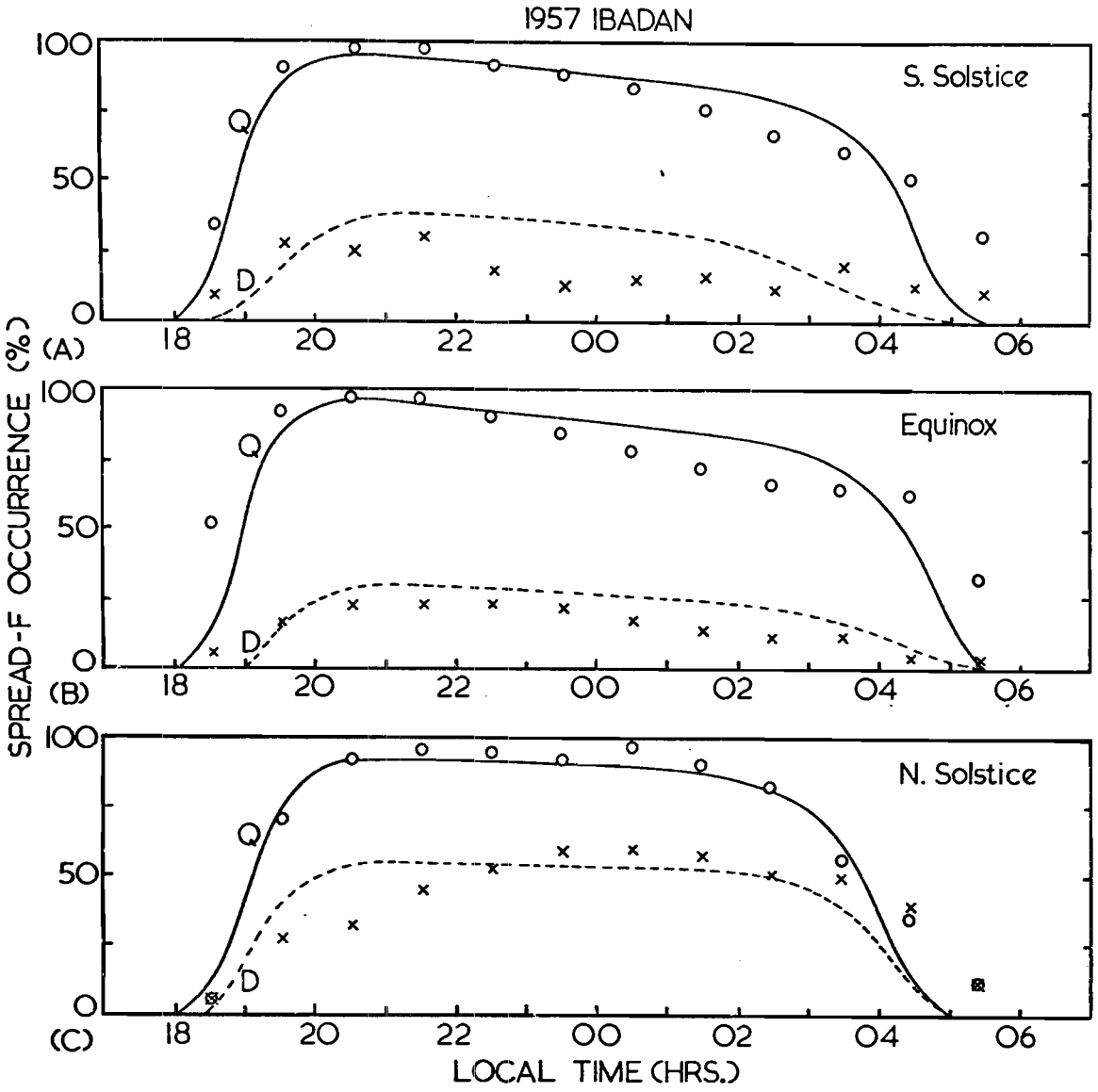

Figure 3. Magnetically quiet and disturbed levels (circles and crosses respectively) of spread-F occurrence at Ibadan in each of the seasons at sunspot maximum. The curves illustrate the modelled distributions.

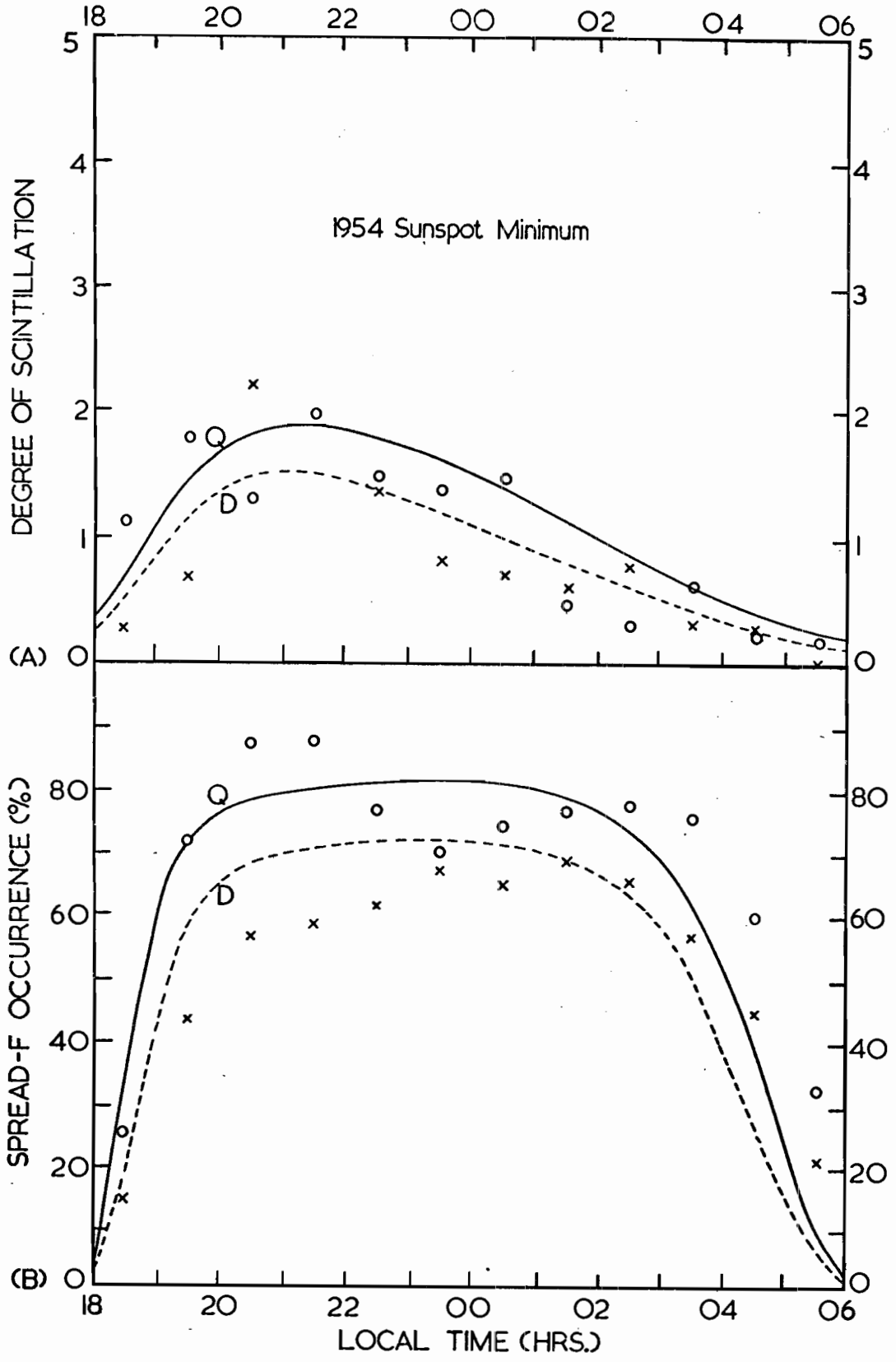

Figure 4. Magnetically quiet and disturbed levels (circles and crosses respectively) of scintillation observed at Accra and spread-F occurrence at Ibadan under sunspot minimum conditions. The curves illustrate the modelled distributions.

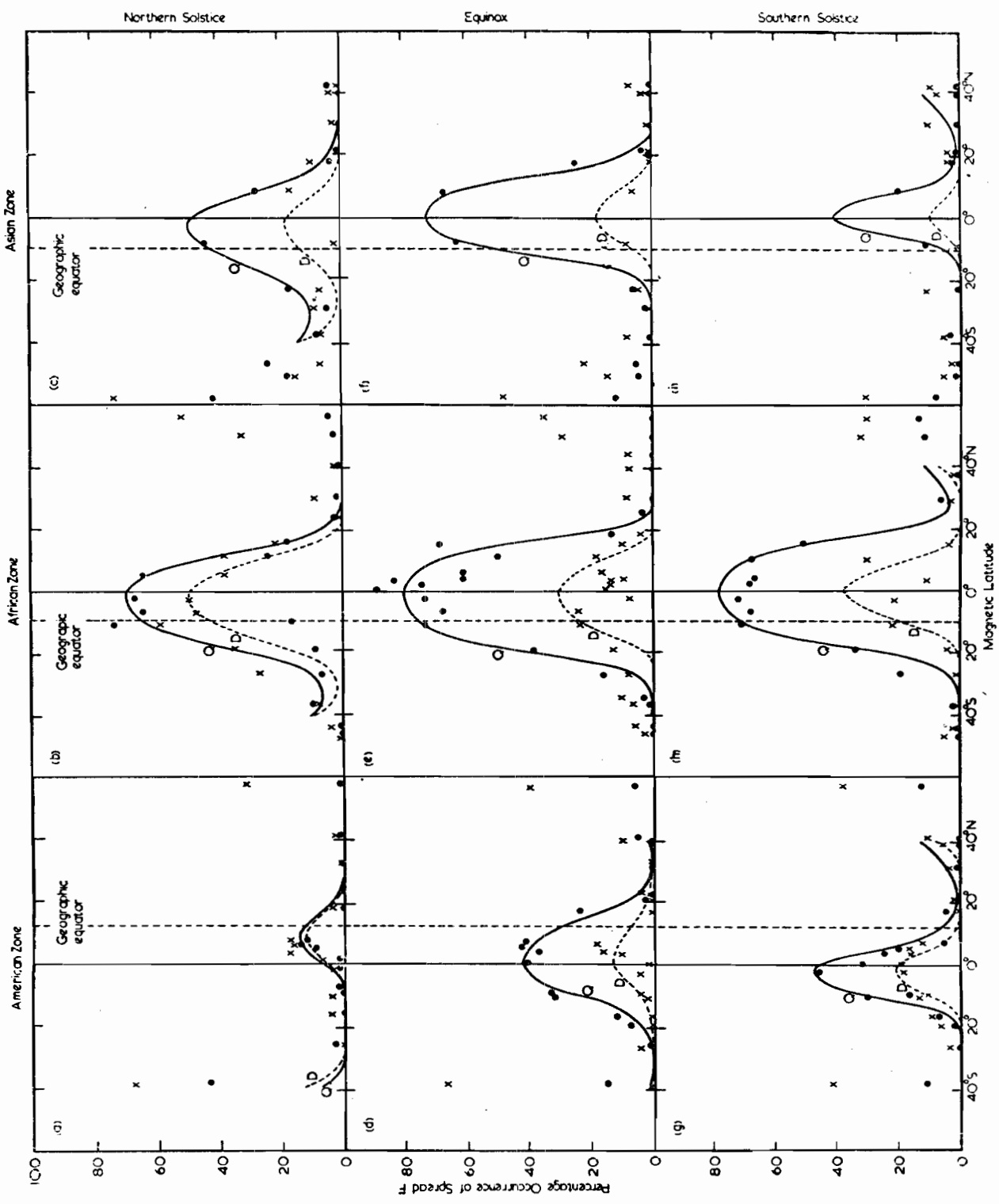

Figure 5. The variation of spread-F occurrence with magnetic latitude for the seasons and longitude zones indicated. The points and crosses refer to magnetically quiet and disturbed conditions respectively. The curves illustrate the modelled distributions.

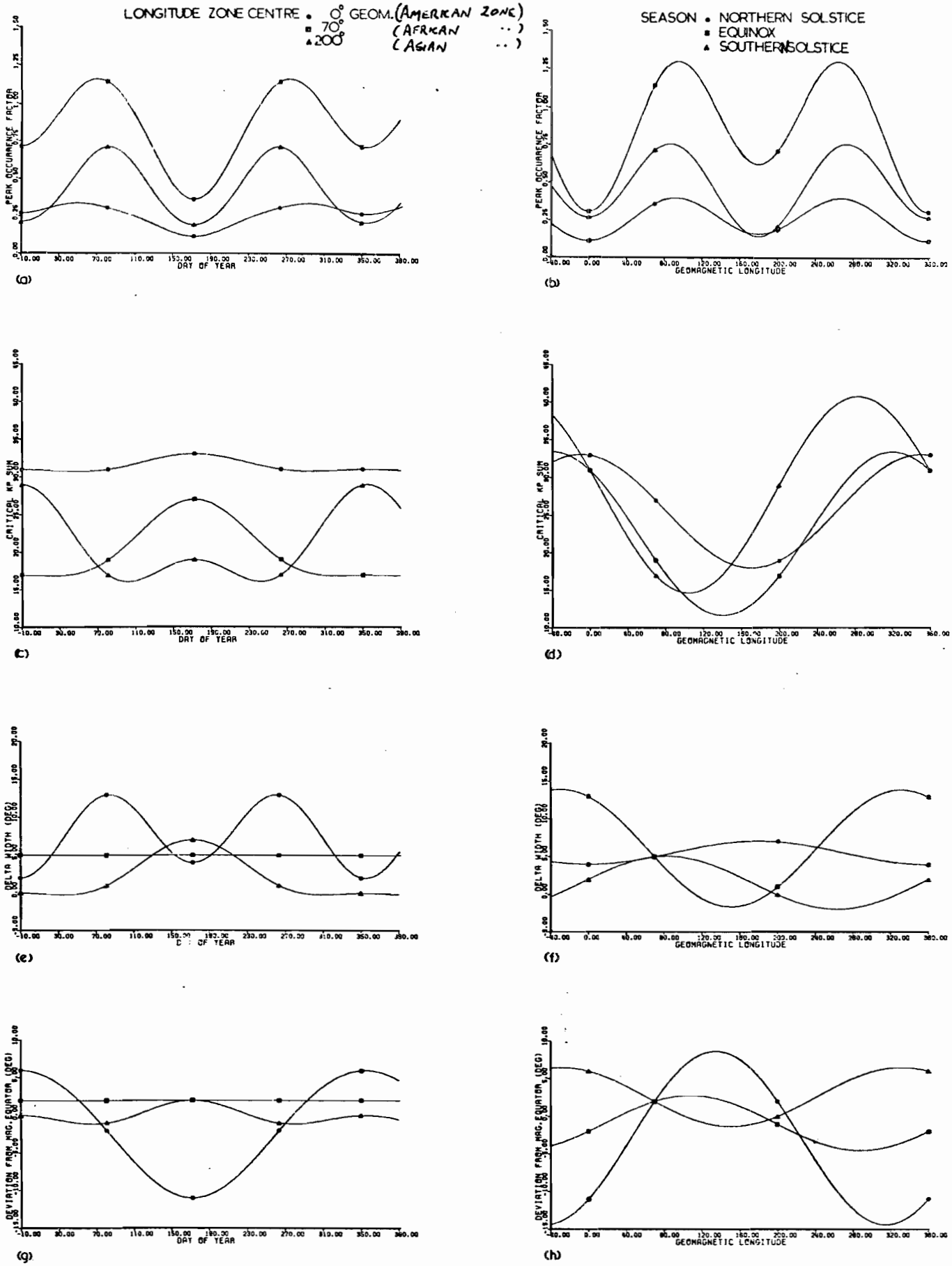

Figure 6. The variation of the peak occurrence factor, critical Kp sum, incremental width and peak position with both the day of year and geomagnetic latitude.

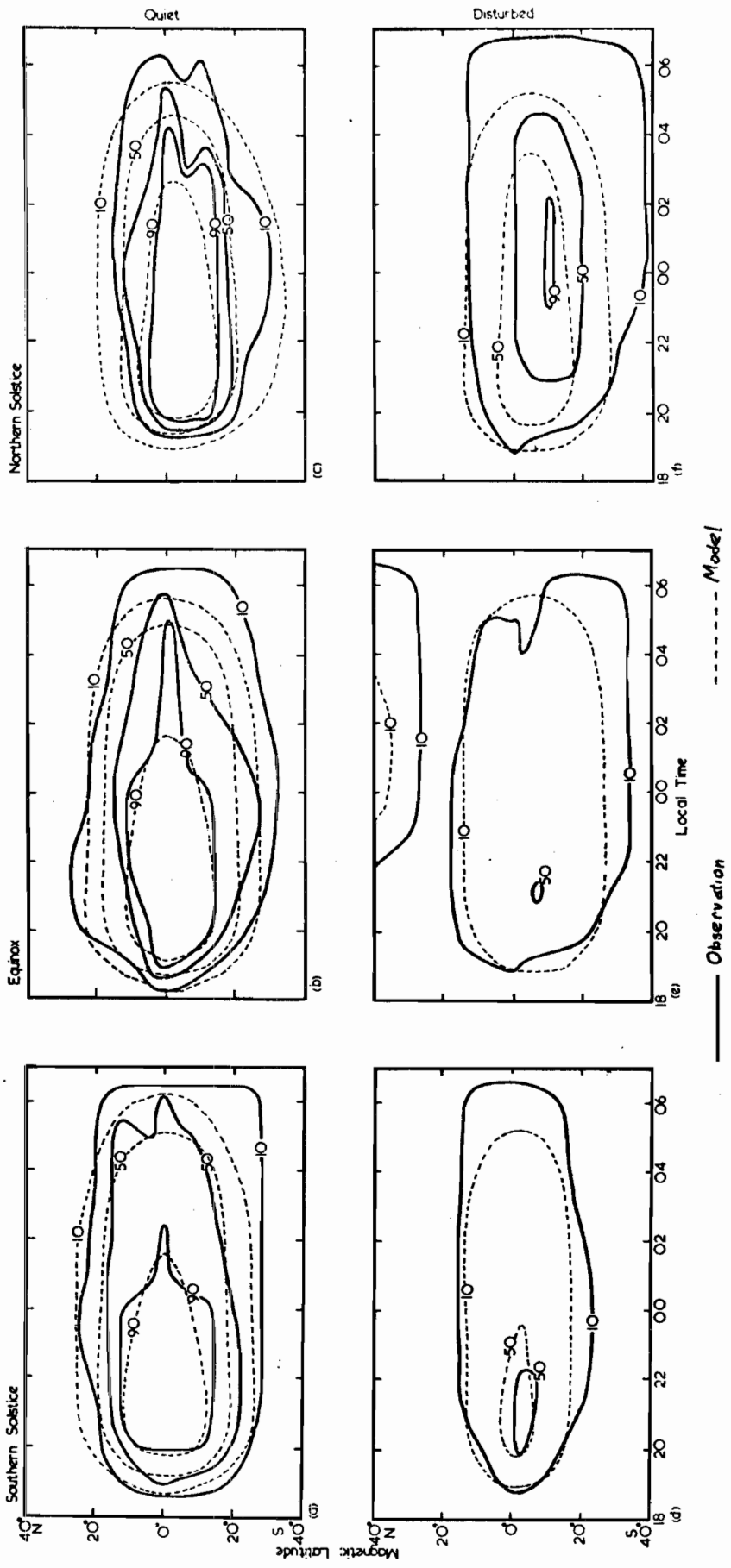

Figure 7. Magnetic latitude versus local time contour plots of spread-F occurrence for the African zone during each of the seasons and magnetically quiet and disturbed conditions.

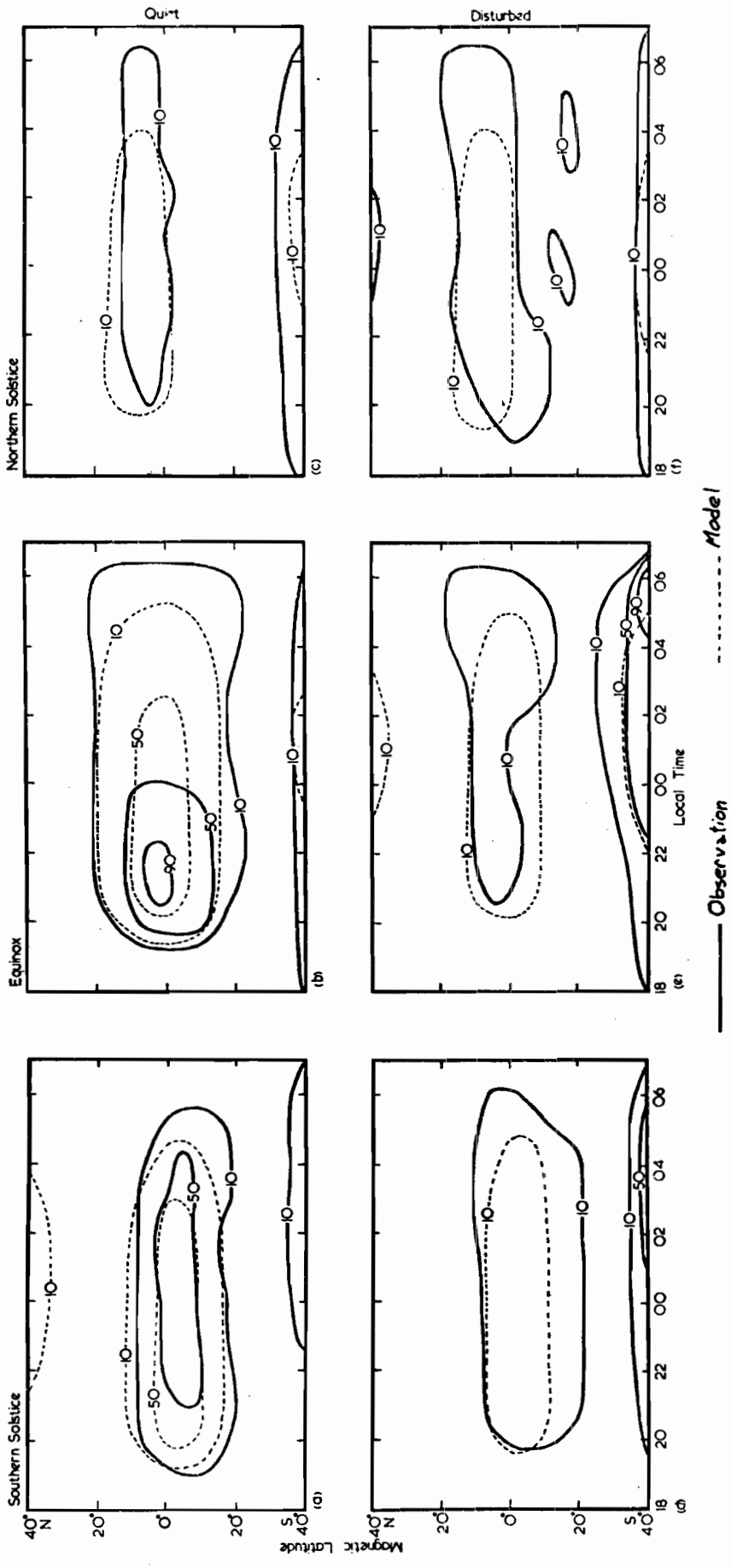

Figure 8. Magnetic latitude versus local time contour plots of spread-F occurrence for the American zone during each of the seasons and magnetically quiet and disturbed conditions.

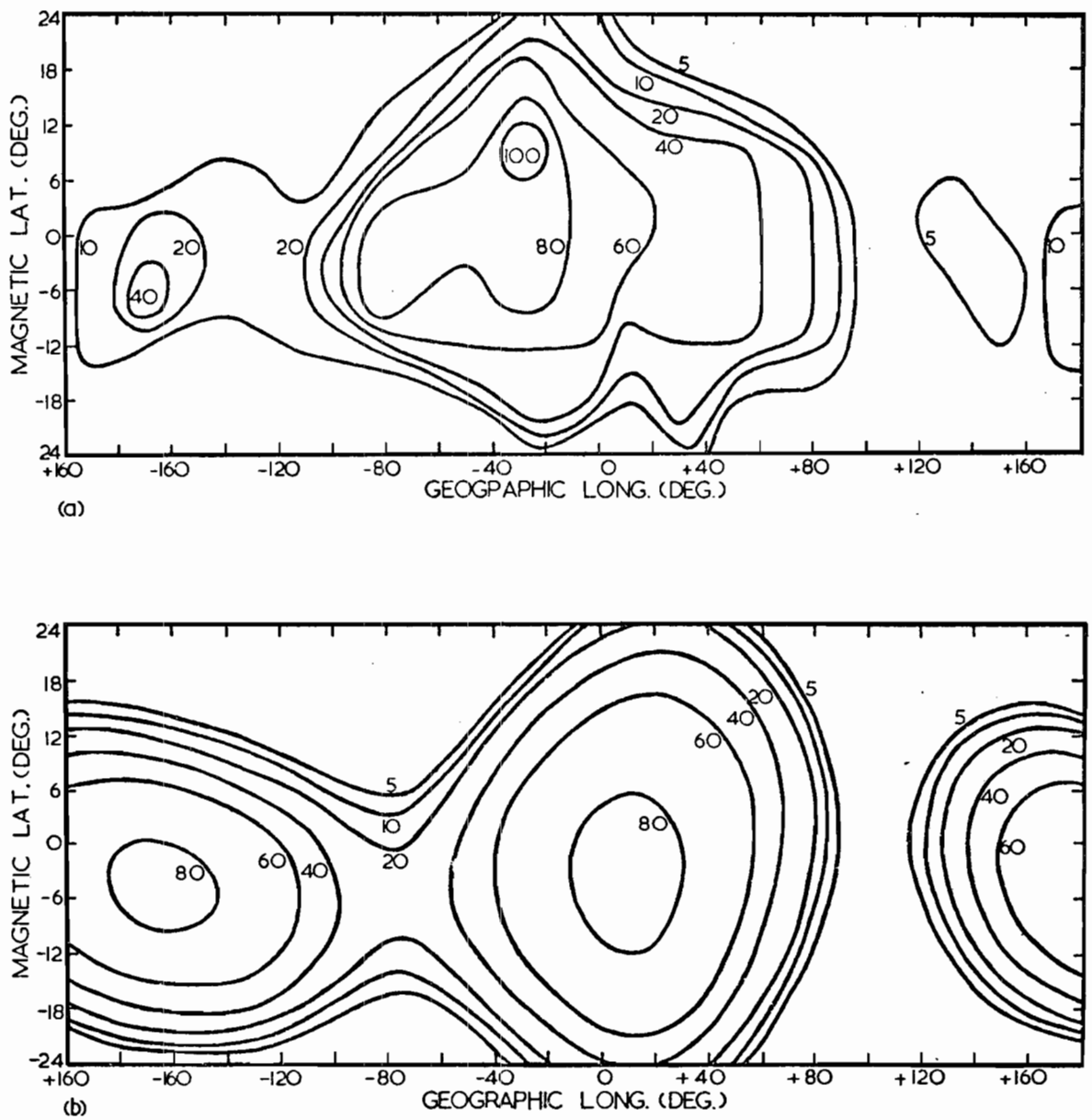

Figure 9. Estimates of the occurrence of scintillations > 4.5 dB over the equatorial region based on (a) OGO-6 data and (b) the irregularity model.

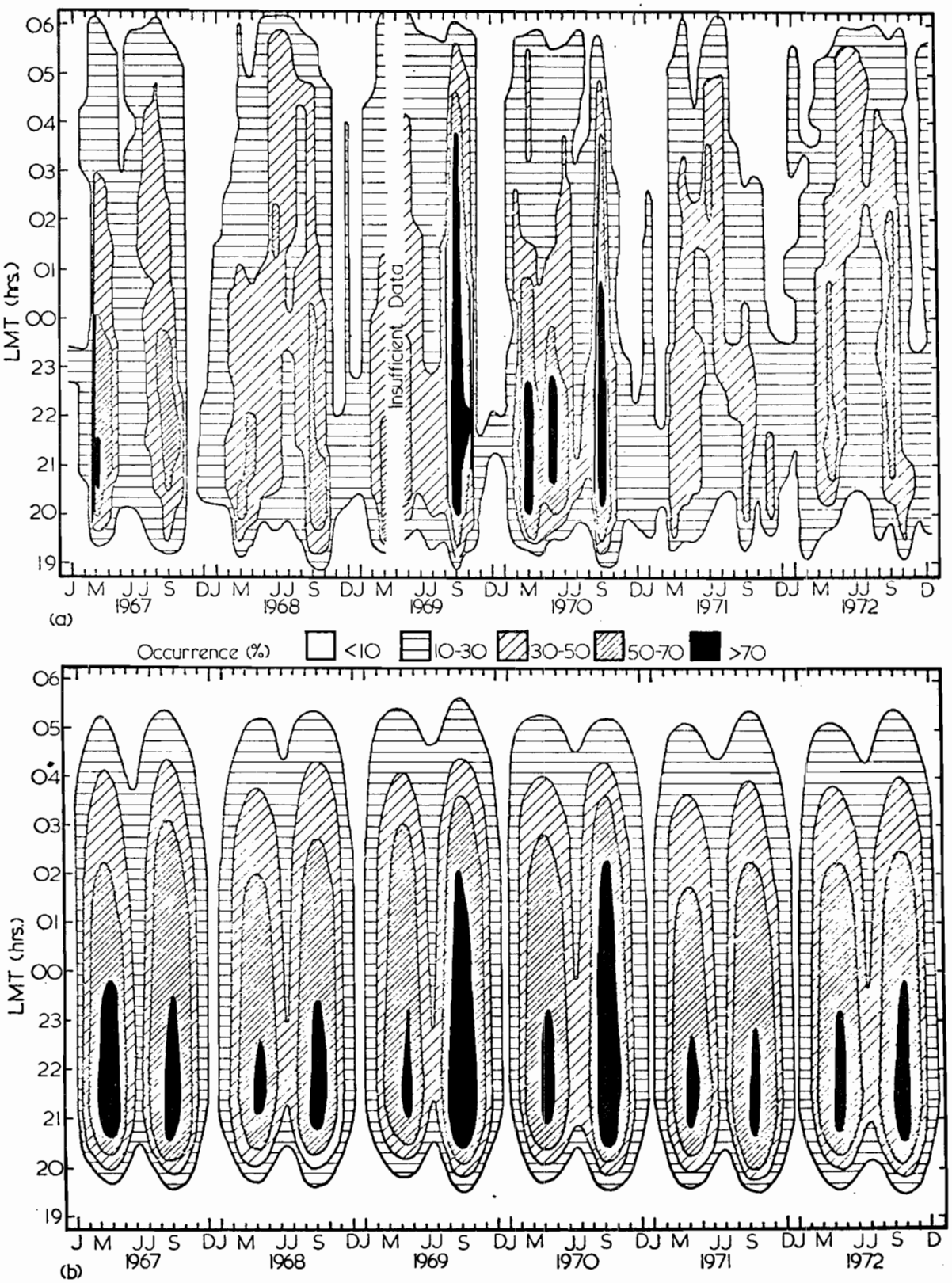

Figure 10. Contour plots of the monthly percentage-occurrence rates of spread-F at Vanimo as a function of local time and month of year.

DOCUMENT CONTROL DATA SHEET

Security classification of this page: UNCLASSIFIED

1 DOCUMENT NUMBERS	
AR Number:	AR-001-415
Report Number:	ERL-0046-TR
Other Numbers:	

2 SECURITY CLASSIFICATION	
a. Complete Document:	UNCLASSIFIED
b. Title in Isolation:	UNCLASSIFIED
c. Summary in Isolation:	UNCLASSIFIED

3 TITLE

AN IMPROVED IONOSPHERIC IRREGULARITY MODEL

4 PERSONAL AUTHOR(S):

D.G. Singleton

5 DOCUMENT DATE:

November 1978

6 6.1 TOTAL NUMBER OF PAGES 40

6.2 NUMBER OF REFERENCES: 39

7 7.1 CORPORATE AUTHOR(S):

Electronics Research Laboratory

7.2 DOCUMENT SERIES AND NUMBER

Electronics Research Laboratory 0046-TR

8 REFERENCE NUMBERS

a. Task: DST 76/10

b. Sponsoring Agency:

9 COST CODE: 137 AA 122

10 IMPRINT (Publishing organisation)

Defence Research Centre Salisbury

11 COMPUTER PROGRAM(S) (Title(s) and language(s))

12 RELEASE LIMITATIONS (of the document):

Approved for Public Release

12.0	OVERSEAS	NO		P.R.	1	A		B		C		D		E	

Security classification of this page: UNCLASSIFIED

Security classification of this page: UNCLASSIFIED

13 ANNOUNCEMENT LIMITATIONS (of the information on these pages):

No Limitation

14 DESCRIPTORS:

a. EJC Thesaurus Terms

Spread F
Scintillation
Electron density (concentration)
Ionosphere
F region
Models
Ionospheric disturbances
Ionospherics
Magnetic disturbances

b. Non-Thesaurus Terms

15 COSATI CODES:

0401

16 LIBRARY LOCATION CODES (for libraries listed in the distribution):

SW SR SD AACA

17 SUMMARY OR ABSTRACT:
(if this is security classified, the announcement of this report will be similarly classified)

Modifications are made to the global model developed by Fremouw et al. for the incremental electron density of F-layer irregularities in order to force the model into agreement with a considerable body of scintillation and spread-F data. While special attention is given to the equatorial region, where the original model was particularly lacking, the results of other studies are used to update the model in the other latitude regions and so provide a model of general application. The model now embodies the effect of magnetic activity at all latitudes, variations of occurrence with longitude in the equatorial region, variability of the width and position of the equatorial region, the influence of irregularity layer thickness, irregularity shape and electron density power spectrum, as well as the diurnal, seasonal and sunspot cycle variations of irregularity occurrence and strength at all latitudes. The improvements proposed not only enhance the model's usefulness as a simulation technique in engineering applications, but should also provide an impetus to the understanding of the physics of the irregularities.

Security classification of this page: UNCLASSIFIED